The stoichiometry of minor-to-major pilins regulates the dynamic activity of the type IVa competence pilus in *Vibrio cholerae*

Nicholas D. Christman, Triana N. Dalia, Jennifer L. Chlebek, and Ankur B. Dalia*

Department of Biology, Indiana University, Bloomington, Indiana, United States of America
*Author for correspondence: ankdalia@iu.edu

ABSTRACT

Type IVa pili (T4aP) are bacterial surface appendages that perform various functions including twitching motility, surface attachment, cell-cell interactions, and DNA uptake for natural transformation. Pivotal to each of these functions is the ability of T4aP to be dynamically extended and retracted from the cell surface. However, the factors that regulate this dynamic activity remain poorly understood. To address this question, we employ the competence T4aP from *Vibrio cholerae* as a model system. T4aP are composed of major and minor pilin subunits, named based on their relative abundance in the pilus filament. Prior work has established that minor pilins form a complex that initiates T4aP assembly. This allows for the subsequent addition of major pilins to the filament, which promotes T4aP extension. Here, we uncover that the stoichiometry of minor-to-major pilins is a crucial determinant of T4aP dynamic activity. Specifically, we show that either (1) overexpressing minor pilins or (2) underexpressing the major pilin results is a dramatic increase in the frequency of T4aP dynamics. These results indicate that the stoichiometry of major-to-minor pilins, not their absolute abundance, is one mechanism that regulates T4aP dynamic activity.

AUTHOR SUMMARY

Type IVa pili (T4aP) are a broadly conserved family of filamentous bacterial appendages that help bacteria colonize surfaces, move towards or away from stimuli, and gain new traits through a mechanism of horizontal gene transfer called natural transformation. T4aP are primarily composed of protein subunits called major and minor pilins, named based on their relative abundance in the pilus filament. Bacteria can dynamically extend and retract pilus filaments from their surface through polymerization and depolymerization of these pilins. This dynamic activity is critical for the activities that T4aP carry out. However, the factors that regulate this dynamic activity remain incompletely understood. Here, we find that the ratio of minor-to-major pilins is one factor that regulates the frequency of dynamic activity. Minor pilins are a universally conserved feature of T4aP. So, the minor-to-major pilin ratio may be a broadly conserved mechanism for controlling dynamic T4aP activity in diverse bacterial species.

INTRODUCTION

Type IV pili (T4aP) are dynamic filamentous nanomachines found in diverse bacteria and archaea that are primarily composed of a repeating protein subunit known as the major pilin [1-3]. However, T4aP filaments also include additional, low abundance pilin proteins known as minor pilins that are crucial for T4aP assembly and function.

Minor pilins play at least two roles in T4aP biology. First, a subset of “core” minor pilins (commonly 4 distinct pilins) form a complex that primes the T4aP machine for filament assembly, and without them, pili are rarely extended [4-7]. As a result, this complex of core minor pilins is likely at the tip of extended pili [4, 7-10]. Second, minor pilins have been shown to

mediate many of the functions of T4aP, namely attachment to surfaces (for twitching motility or biofilm formation), cell-cell interactions, and DNA-binding for natural transformation [8-16]. These activities can be attributed to core and auxiliary minor pilins, depending on the T4aP system. In addition to the tip-associated minor pilin complex, minor pilins may also be inserted along the length of pili [17, 18].

Critical to T4aP function is the ability of individual T4aP machines to actively extend and retract a pilus, a property we define as "dynamic activity" [19]. While dynamic activity is a necessary property of T4aP, not all systems exhibit the same frequency of dynamic activity [8, 20-24]. One possibility is that the frequency of dynamic activity is optimized for the function that each T4aP carries out. Despite dynamic activity being crucial for T4aP function, the factors that regulate this dynamic activity remain poorly understood in most systems. Here, we use the competence T4aP from *V. cholerae*, an emerging model system for studying T4aP dynamics [8, 20, 25-31], to address this question.

RESULTS

Overexpression of minor pilins increases the frequency of T4aP dynamic activity

V. cholerae competence T4aP dynamics can be directly observed by epifluorescence timelapse microscopy using strains where the major pilin, *pilA*, contains a cysteine knock-in ($pilA^{S67C}$) that allows for labeling pili with an Alexa Fluor 488 conjugated maleimide dye (AF488-mal) [8, 28]. In the parent strain, competence T4aP are rapidly extended and retracted; and the majority of cells exhibit ≤2 dynamic pili during a 2 min timelapse (**Fig. 1A-C**) [8, 31]. However, each cell has the capacity to assemble many more pili. This is supported, in part, by the observation that deletion of the retraction motor ATPase, *pilT*, results in hyperpiliated cells (**Fig. S1**) [8, 20, 25, 26, 30]. This suggests that the frequency of dynamic activity is constrained in the parent.

Because core minor pilins are essential for initiating pilus assembly, we hypothesized that a low abundance of core minor pilins may be one factor that constrains the frequency of dynamic activity (**Fig. 1A-C**). To test this, we first needed to establish the identity of the core pilins of the *V. cholerae* competence T4aP. It was previously hypothesized that VC0858, VC0859, VC0860, and VC0861 encode the competence T4aP minor pilins [30]. Furthermore, recent work has established that diverse members of the type IV filament family contain a structurally conserved core of 4 minor pilins that initiate pilus assembly [4, 5, 7, 9, 32]. AlphaFold modeling suggests that the minor pilins encoded by VC0858-VC0861 form this initiation complex (**Fig. S2**). To reflect this conservation and to ease comparisons between T4aP systems, we have named these putative minor pilins based on the convention established in *Myxococcus xanthus* and *Pseudomonas aeruginosa*: VC0858 = *fimT*, VC0859 = *pilW*, VC0860 = *pilX*, and VC0861 = *pilV*.

Because core minor pilins prime T4aP extension, deletion of minor pilin genes results in a severe reduction in pilus assembly. Pilus assembly in minor pilin mutants, however, is not completely eliminated [4, 33-35], which is likely due to cross-complementation via the minor pilins of the type II secretion system [6]. Thus, we mutated each of the four putative minor pilin genes to test whether they exhibited the characteristic phenotype of reduced, but not eliminated, surface piliation. For these experiments, we utilized a Δ*pilT* background to sensitize the assay and to easily assess pilus assembly in static images (*i.e.*, assembled pili will remain static on the cell surface in the Δ*pilT* background). Mutating *fimT*, *pilW*, *pilX*, and *pilV*, severely reduced, but did not eliminate, surface piliation (**Fig. S1**), which is consistent with them encoding the core minor pilins. By contrast, mutating the essential competence T4aP machine component *pilQ* [30, 36] results in a complete loss in surface piliation (**Fig. S1**). Importantly, the surface piliation of each minor pilin mutant could be complemented (**Fig. S1**).

Next, we sought to test whether the abundance of these minor pilins regulates dynamic activity. We hypothesized that if low expression of minor pilins constrains dynamic activity, then overexpression of these minor pilins should markedly increase the frequency of T4aP dynamics. The native *fimT*, *pilW*, *pilX*, and *pilV* genes are all expressed in an operon; and these genes are partially overlapping, which indicates that they are likely translationally coupled [37, 38] to maintain expression at a fixed stoichiometry. To overexpress these core minor pilins while preserving their translational coupling, we cloned the entire *fimT-pilW-pilX-pilV* operon (TWXV) downstream of an IPTG-inducible promoter (P_{tac}-TWXV) and integrated this construct at an ectopic site. To assess the degree of overexpression, we generated a functional internally FLAG-tagged allele of PilX (*pilX*::FLAG) (**Fig. S3A**) to assess the relative expression level of minor pilins. Semi-quantitative western blots (**Fig. S4A-B**) of native *pilX*::FLAG vs *pilX*::FLAG P_{tac}-TWX(::FLAG)V indicates that minor pilins are overexpressed in the latter (**Fig. 1D**). Notably, while the *pilX*::FLAG allele is functional for natural transformation (**Fig. S3A**), it exhibits a slight reduction in dynamic activity (**Fig. S3B-D**), which limits the sensitivity of these assays. As a result, all functional assays utilized strains with untagged *pilX*.

To determine whether minor pilin abundance regulates T4aP, we next assessed pilus dynamic activity in P_{tac}-TWXV and found that the frequency of dynamic activity was dramatically increased compared to the parent (**Fig. 1A-C)**. Importantly, P_{tac}-TWXV did not markedly affect other properties of T4aP dynamics including pilus length, retraction rate, or the dwell time between extension/retraction (**Fig. S5A-C**). While a very modest, but significant, reduction was observed on T4aP extension rates (**Fig. S5D**), this difference is unlikely to explain the large increase in the frequency of dynamic activity observed. Together, these data strongly suggest that overexpression of the minor pilins increases the frequency of T4aP dynamic activity.

Thus far, we have only assessed the frequency of T4aP dynamics through direct observation. Competence T4aP dynamic activity promotes the uptake of DNA across the outer membrane during natural transformation [8, 30]. Thus, if minor pilin overexpression increases the frequency of T4aP dynamic activity, we hypothesized that the rate of DNA uptake should increase in cells overexpressing minor pilins. To test this, we used a qPCR-based DNA uptake assay as a functional readout for T4aP dynamic activity. In brief, cells were incubated with a tDNA PCR product that contains a sequence that is unique from the host genome. At defined timepoints, aliquots of the reaction were removed and mixed with DNase I to degrade extracellular DNA and to prevent further tDNA uptake. Importantly, tDNA taken up across the outer membrane via competence T4aP dynamic activity is protected from degradation. DNase treated aliquots were then boiled (to inactivate the DNase and to release periplasmic tDNA via cell lysis) and used as template for qPCR reactions to detect the abundance of the tDNA product (see **Methods** for details). Altogether, this approach allowed us to kinetically monitor DNA uptake across the outer membrane (**Fig. 1E**). The line of best fit was determined by linear regression analysis to define the slope, which represents the rate of DNA uptake (**Fig. 1E-F**). Importantly, a strain incapable of assembling competence T4aP (Δ*pilA*) lacked any measurable uptake, which indicates that the tDNA uptake observed in this assay is dependent on T4aP dynamics. When we tested P_{tac}-TWXV, we found that this strain exhibits a significant increase in the rate of DNA uptake compared to the parent (**Fig. 1E-F**). These results reinforce that overexpression of minor pilins dramatically increases the frequency of T4aP dynamics.

These results are consistent with a model wherein T4aP dynamics are constrained in the parent due to a limited supply of the minor pilin complexes needed to initiate T4aP assembly. Minor pilins and major pilins, however, are structurally similar and it is possible that these proteins compete with one another to gain access to the T4aP machine. Thus, a distinct possibility is that

153 it is not the absolute abundance of minor pilins, but rather the stoichiometric ratio of minor:major
154 pilins that regulates dynamic activity. Overexpression of the minor pilins does not alter the
155 absolute abundance of PilA, as determined by semi-quantitative western blots (**Fig. 1D, S4C-D**).
156 Thus, overexpression of minor pilins via P_{tac}-YWXV increases both the absolute abundance of
157 minor pilins and the ratio of minor:major pilins, which prevents us from distinguishing between
158 these two models.
159
160 *The stoichiometry of minor:major pilins regulates the frequency of T4aP dynamic activity*
161 Next, we sought to increase the minor:major pilin ratio without increasing the absolute
162 abundance of minor pilins to help discriminate between these two models. To do this, we sought
163 to underexpress the major pilin while maintaining expression of minor pilins at their native level.
164 If it is the low absolute abundance of minor pilins that constrains T4aP dynamic activity, this
165 perturbation should have a limited effect on the frequency of T4aP dynamics. However, if it is
166 the ratio of minor:major pilins that regulates T4aP dynamics, then underexpression of the major
167 pilin should increase the frequency of T4aP dynamics in a manner that phenotypically
168 resembles overexpression of the minor pilins.
169
170 To test this hypothesis, we generated a strain with an in-frame deletion of the major pilin, *pilA*,
171 and expressed *pilA in trans* via an IPTG-inducible P_{tac} promoter (pMMB::P_{tac}-*pilA*). To assess
172 whether this genetic background allows for titratable control of PilA expression without affecting
173 expression of the minor pilins, we performed semi-quantitative western blots. These
174 experiments showed that PilA levels were titratable in this background; with 50 μM IPTG
175 inducing native levels of PilA, and lower concentrations of IPTG yielding underexpression of PilA
176 (**Fig. 2A, S4C-D**). Importantly, minor pilin expression is unaffected in this background as levels
177 of PilX::FLAG were indistinguishable from the parent regardless of IPTG concentration (**Fig. 2A,**
178 **Fig. S4B-C**). These results indicate that the Δ*pilA* pMMB::P_{tac}-*pilA* background will allow us to
179 test our hypothesis because at concentrations of IPTG <50 μM the ratio of minor:major pilins is
180 increased, while the absolute abundance of minor pilins is unchanged.
181
182 If PilA is expressed at parent levels in this background (50 μM IPTG), the frequency of T4aP
183 dynamic activity is indistinguishable from the parent (**Fig. 2B**). Underexpression of PilA in this
184 background (10 μM - 40 μM IPTG), however, results in a progressive increase in the frequency
185 of observable T4aP dynamic activity (**Fig. 2B, Fig. S6A**). Furthermore, when PilA is
186 underexpressed using 10 μM IPTG, the relative ratio of minor:major pilins is similar to when
187 minor pilins are overexpressed (**Fig. S7A**); and the frequency of T4aP dynamics is statistically
188 indistinguishable between these conditions (**Fig. S7B**). Importantly, underexpression of PilA
189 does not affect pilus length, retraction rate, or the dwell time between extension/retraction; and
190 only modestly decreases the extension rate (**Fig. S5**), which is consistent with what is observed
191 when minor pilins are overexpressed (**Fig. S5**). Furthermore, the increase in T4aP dynamics
192 observed is directly correlated with a functional increase in the rate of DNA uptake (**Fig. 2C-D,**
193 **Fig. S6B**). Altogether, these data strongly suggest that the minor:major pilin ratio, not the
194 absolute abundance of minor pilins, regulates the frequency of T4aP dynamic activity.
195
196
197 **DISCUSSION**
198 This study sheds light on a mechanism used to regulate dynamic activity in T4aP systems.
199 Specifically, we show that the stoichiometric ratio of minor:major pilins, not their absolute
200 abundance, regulates the frequency of competence T4aP dynamics in *V. cholerae*. The
201 molecular mechanism underlying this regulation is unclear, however we suggest two
202 possibilities. The core minor pilins likely interact with one another to form initiation complexes in
203 the membrane, thus, one possibility is that a high minor:major pilin ratio simply increases the

likelihood that initiation complexes will form; while a low minor:major pilin ratio disrupts assembly due to the inappropriate incorporation of the major pilin into nascent initiation complexes. Following the formation of initiation complexes, the minor pilins must interact with the T4P machine to prime filament extension. So a second possibility is that a higher minor:major pilin ratio allows initiation complexes to more successfully compete with the major pilin for access to the T4P machine, thus, priming more T4P machines for extension. Distinguishing between these two possibilities is experimentally challenging, but represents one focus of future work.

Our findings add to a growing list of factors that have been shown to influence the frequency of T4aP dynamics in diverse bacterial species. In some T4aP systems, the activity of the extension motor ATPase is allosterically regulated, either directly or indirectly, via the secondary messenger cyclic-di-GMP [39-43]. The extension and retraction motor ATPases may also antagonistically compete for the T4aP machine in *P. aeruginosa* [44], suggesting that the ratio of motor ATPases can alter dynamic activity. Also, T4aP dynamics are spatially and temporally regulated in many systems, especially for twitching motility. This includes regulation of twitching motility by a chemosensory system in *P. aeruginosa* [22, 45], phototaxis in cyanobacteria [46], and the control of social motility in *M. xanthus* [47]. Here, we show that the minor:major pilin ratio can also influence the frequency of T4aP dynamics. The core minor pilins that initiate pilus assembly are a universally conserved feature of T4aP. Thus, it is tempting to speculate that the minor:major pilin ratio affects the dynamic activity of T4aP in other species. Also, many species encode the PilS/PilR two-component system that transcriptionally regulates the expression of the major pilin based on the pilin load of the inner membrane [48-52]. This could help stabilize minor:major pilin ratios for consistent dynamic activity; or perhaps more speculatively, could provide a mechanism for altering minor:major pilin ratios to tune dynamic activity based on environmental cues. Notably, *V. cholerae* lacks PilS/PilR; and our results demonstrate that expression of the competence T4aP minor and major pilins is uncoupled, which allowed us to easily manipulate the relative minor:major pilin ratio in this study.

Our findings add to a growing list of factors that regulate the frequency of T4aP dynamics. Other properties of T4aP dynamics include the rate of extension/retraction, the length of pili, and the dwell time between extension/retraction. Prior work has shown that extension/retraction rates are defined, in part, by the ATP hydrolysis rate of the motor ATPases that power extension/retraction, respectively [20, 23, 27, 53]. We show here that the minor:major pilin ratio also has a slight, but significant, negative effect on extension rates; however, a mechanistic understanding for this observation remains lacking. Also, the factors that define pilus length and the switch between extension and retraction remain poorly understood in T4aP systems, which will be the focus of future work.

Our results highlight that the frequency of competence T4aP dynamics are constrained in *V. cholerae*. But why would bacteria want to constrain the dynamic activity of their T4aP? Our results show that increasing T4aP dynamics can increase the rate of DNA uptake for the competence T4aP in *V. cholerae*. Thus, increased T4aP dynamics can clearly benefit cells by enhancing their capacity for horizontal gene transfer by natural transformation. On the other hand, increased T4aP dynamics may incur a fitness cost. First, T4aP dynamics are likely energetically costly, so increased dynamics could drain cellular resources. Also, T4aP are common phage receptors. So increased T4aP dynamics can increase the vulnerability to phage infection. One way bacteria can mitigate this vulnerability is by reducing the frequency of T4aP dynamics [43]. Also, recent studies highlight that prophages decrease T4aP dynamics as a mechanism of superinfection exclusion [54, 55], which further suggests that constraining T4aP dynamics can promote phage resistance. Finally, there may be environmental conditions where

255 T4aP-dependent activities are disadvantageous. For example, retraction of MSHA T4aP and
256 cessation of dynamics can promote escape from environmental stressors [29], and enhance
257 colonization of mammalian hosts [56] in *V. cholerae*. We find here that T4aP dynamics are
258 influenced, in part, by the ratio of minor:major pilins. This simple regulatory mechanism may
259 allow bacteria to rapidly optimize T4aP dynamics to balance the associated costs and benefits.
260
261
262 **METHODS**
263 *Bacterial strains and culture conditions*
264 All *V. cholerae* strains were derived from *V. cholerae* E7946 [57]. Cells were routinely grown in
265 LB Miller broth rolling at 30 ºC or on LB miller agar at 30 ºC supplemented with trimethoprim (10
266 µg/mL), spectinomycin (200 µg/mL), kanamycin (50 µg/mL), tetracycline (0.5 µg/mL),
267 erythromycin (10 µg/mL), chloramphenicol (1 µg/mL), carbenicillin (100 µg/mL) or zeocin (100
268 µg/mL) as appropriate.
269
270 In order to isolate and study dynamic activity of the competence T4aP in *V. cholerae*, the parent
271 strain used throughout this study had several critical mutations: 1) Expression of competence
272 T4aP naturally requires chitin oligosaccharides and quorum sensing as inducing cues. To
273 reliably study T4aP dynamics, we bypassed these native signals by overexpressing the master
274 regulator of competence, TfoX, via a constitutively active promoter, P_{const2}, and deleted *luxO* to
275 genetically lock cells in a high density state as previously described [8]. 2) To detect active T4aP
276 using fluorescence microscopy, all strains harbored a $pilA^{S67C}$ mutation which allows for pilus
277 labeling with fluorescent maleimide dyes [8, 28]. 3) *V. cholerae* strains naturally encode two
278 plasmid defense systems, *ddmABC* and *ddmDE*, that can deplete cells of plasmids used for
279 ectopic complementation [58]. To use pMMB::P_{tac}-*pilA* in the absence of antibiotics, these two
280 plasmid defense systems were deleted.
281
282 *Construction of mutant strains*
283 All strains were generated by natural transformation using mutant constructs assembled by
284 splicing-by-overlap extension (SOE) exactly as previously described [59, 60] and confirmed by
285 PCR and sequencing. For a detailed list of strains used for this study, see **Table S1**. For a
286 complete list of primers used to generate mutant constructs, see **Table S2**.
287
288 The pMMB::P_{tac}-*pilA* plasmid was assembled by SOE PCR and cloned into chemically
289 competent *Escherichia coli* TG1. This plasmid was then miniprepped and introduced into *V.*
290 *cholerae* via natural transformation.
291
292 *Direct visualization of competence T4aP by epifluorescence microscopy*
293 To prepare cells for imaging, cultures were grown at 30 ºC rolling in LB supplemented with 100
294 µM IPTG, 20 mM $MgCl_2$, 10 mM $CaCl_2$ to late log. Then, ~10^8 cells were harvested and washed
295 in instant ocean medium (IO; 7g/L, Aquarium Systems) to remove residual LB. To label
296 competence T4aP, washed cells were incubated with 25 ng/mL AlexaFluor 488-maleimide
297 (AF488-mal) dye (ThermoFisher) for 20-30 mins at room temperature. To remove unbound dye,
298 cells were washed three times in IO. Then, cells were placed under a 0.4% gelzan pad for
299 imaging. Phase contrast and widefield fluorescence images were collected using a Nikon Ti-2
300 microscope using a Plan Apo × 60 objective, a FITC filter cube, a Hamamatsu ORCA Flash 4.0
301 camera and Nikon NIS Elements imaging software. For timelapse imaging, samples were
302 incubated at 30 ºC using an adjustable objective warmer (Bioptechs Inc.).
303
304 *Microscopy image analysis*

305 To assess surface piliation in Δ*pilT* strains, static images were taken of AF488-mal labeled cells.
306 Fiji imaging software [61] with the microbeJ plugin [62] was used to quantify the number of cells
307 in a field of view. Then, the fields of view were visually scanned to quantify the number of cells
308 with rare piliation events (in the case of the minor pilin deletion mutants) or rare non-piliated
309 cells (in the case of the Δ*pilT* parent or minor pilin complemented strains).
310
311 To quantify the frequency of dynamic activity, timelapse microscopy was performed by imaging
312 AF488-mal labeled cells every 3 sec for 2 mins. Samples were incubated at 30 ºC for the
313 duration of the timelapse. Timelapse images were analyzed using NIS elements software. For
314 each replicate, 60 cells were randomly selected using the phase contrast channel. For each cell,
315 the fluorescence channel was then manually analyzed to determine the number of extension
316 and/or retraction events observed. Every dynamic pilus observed within the 2 min timelapse
317 was scored as a distinct dynamic event. We have found empirically that pili < 0.15 µm cannot be
318 resolved via this imaging approach.
319
320 The maximum length of dynamic competence T4aP was measured using the same timelapse
321 images used to quantify dynamic activity. NIS elements software was used and cells in a field of
322 view were analyzed one-by-one for piliation events during the 2 min timelapse. When a pilus
323 was observed, it's maximum length was measured using the multi-point tool to account for the
324 flexibility of T4aP.
325
326 To measure extension rates, retraction rates, and dwell times, timelapse microscopy was
327 performed by imaging AF488-mal labeled cells every 1 sec for 1 min. Cells were visually
328 assessed to identify pili that completely extended and retracted during the course of the
329 timelapse. The frame and timestamp at the beginning and end of the extension/retraction event
330 was recorded. Also, the maximum pilus length for each dynamic event was measured. Then, the
331 length of the pilus (in µm) was divided by the elapsed time for extension and retraction (in sec)
332 to define the extension rate and retraction rate (µm/s), respectively. The dwell time was defined
333 as the time (in sec) elapsed between when a pilus stopped extending and when retraction
334 began.
335
336 *Semi-quantitative western blot analysis*
337 Strains were grown as described above for microscopy. For PilA, ~$5x10^9$ cells were centrifuged
338 and resuspended in 50 µL IO. This was then mixed 1:1 with 2x SDS-PAGE sample buffer (200
339 mM Tris pH 6.8, 25% glycerol, 4.1% SDS, 0.02% Bromophenol Blue, 5% β-mercaptoethanol)
340 and boiled for 10 mins. Samples were diluted into a Δ*pilA* lysate so that the signal was within
341 the linear range of the assay (see **Fig. S4**), and then electrophoretically separated on a 15%
342 SDS-PAGE gel.
343
344 For PilX::FLAG, ~$5x10^{10}$ cells were centrifuged and resuspended in 50 µL IO. The solution was
345 then mixed with lysis buffer [1x FastBreak lysis buffer (Promega), 3.8 µg/mL lysozyme
346 (GoldBio), and 25 U Benzonase (Sigma Aldrich)] and incubated at room temperature for 10
347 mins. Then, each lysis reaction was mixed 1:1 with 2x SDS-PAGE sample buffer. Samples were
348 then electrophoretically separated on a 15% SDS-PAGE gel. Samples were diluted into a lysate
349 of the parent (no FLAG) so that the signal was within the linear range of the assay (see **Fig.**
350 **S4**).
351
352 Proteins were then electrophoretically transferred to PVDF membranes. To detect PilA, blots
353 were stained with polyclonal α-PilA primary antibodies [26]. To detect PilX::FLAG, blots were
354 stained with monoclonal α-FLAG primary antibodies (Sigma). Blots were then incubated with

HRP-conjugated secondary antibodies, developed using enhanced chemiluminescence (ECL) western blotting substrate (Pierce), and imaged on a ProteinSimple Fluorechem R instrument.

Protein densities were quantified using Fiji imaging software. Serial dilutions of PilX::FLAG and PilA lysates were performed to identify the linear range of detection for these western blots (see **Fig. S4**). Experimental samples were diluted so that their signal density was within the linear range (see **Fig. S4**), and densities were then multiplied by the dilution factor to obtain the signal density of the original sample.

qPCR-based DNA uptake assays

To assess the rate of DNA uptake, cells were grown as described above for microscopy assays. Each DNA uptake reaction consisted of IO, 0.1 mg/mL recombinant BSA (NEB), 2 ng/µL transforming DNA (tDNA; a 300 bp Δ*VC1102* PCR product), and ~$1x10^7$ cells. Each reaction was incubated at 30ºC, and aliquots were taken at 30, 60, 120, 240, and 480 seconds after the addition of tDNA. At each timepoint, the aliquot was immediately added to a DNase solution consisting of IO, 0.1 mg/mL recombinant BSA, 1x DNase buffer (NEB), and 6 units of DNase I (NEB) and mixed by pipetting. After allowing the DNase reaction to proceed at room temperature for 2 mins, samples were boiled and then placed on ice.

Next, each sample was used as template for qPCR on a StepOnePlus instrument (Applied Biosystems). To determine the quantity of tDNA taken up, qPCR was performed with a primer pair that would uniquely detect the tDNA. And to normalize samples, qPCR was also performed for *rpoB* to quantify the number of cells in each aliquot. The tDNA molecules per cell was determined by dividing the quantity of Δ*VC1102* by the quantity of *rpoB*. Then, linear regression analysis was performed to determine the rate of DNA uptake for each strain.

Structural modeling of minor pilins

Proteins were modeled using the AlphaFold-multimer algorithm [63] in ColabFold [64] on Indiana University's high-performance computing (HPC) system. Colabfold runs were configured for 10 recycles with an early stop tolerance of 0.4. Models were analyzed and visualized using UCSF ChimeraX [65].

Statistics

Statistical differences were assessed using GraphPad Prism software. The statistical tests used are indicated in the figure legends. Descriptive statistics for all samples, and a comprehensive list of statistical comparisons can be found in **Dataset S1**.

ACKNOWLEDGEMENTS

This work was supported by Grant R35GM128674 from the NIH to A.B.D.

REFERENCES

1. Craig L, Taylor RK, Pique ME, Adair BD, Arvai AS, Singh M, et al. Type IV pilin structure and assembly: X-ray and EM analyses of Vibrio cholerae toxin-coregulated pilus and Pseudomonas aeruginosa PAK pilin. Mol Cell. 2003;11(5):1139-50. doi: 10.1016/s1097-2765(03)00170-9. PubMed PMID: 12769840.
2. Craig L, Volkmann N, Arvai AS, Pique ME, Yeager M, Egelman EH, Tainer JA. Type IV pilus structure by cryo-electron microscopy and crystallography: implications for pilus assembly and functions. Mol Cell. 2006;23(5):651-62. doi: 10.1016/j.molcel.2006.07.004. PubMed PMID: 16949362.

3. Denise R, Abby SS, Rocha EPC. Diversification of the type IV filament superfamily into machines for adhesion, protein secretion, DNA uptake, and motility. PLOS Biology. 2019;17(7):e3000390. doi: 10.1371/journal.pbio.3000390.
4. Nguyen Y, Sugiman-Marangos S, Harvey H, Bell SD, Charlton CL, Junop MS, Burrows LL. Pseudomonas aeruginosa Minor Pilins Prime Type IVa Pilus Assembly and Promote Surface Display of the PilY1 Adhesin. Journal of Biological Chemistry. 2015;290(1):601-11. doi: 10.1074/jbc.m114.616904.
5. Cisneros DA, Bond PJ, Pugsley AP, Campos M, Francetic O. Minor pseudopilin self-assembly primes type II secretion pseudopilus elongation. The EMBO Journal. 2012;31(4):1041-53. doi: 10.1038/emboj.2011.454.
6. Cisneros DA, Pehau-Arnaudet G, Francetic O. Heterologous assembly of type IV pili by a type II secretion system reveals the role of minor pilins in assembly initiation. Molecular Microbiology. 2012;86(4):805-18. doi: 10.1111/mmi.12033.
7. Treuner-Lange A, Chang Y-W, Glatter T, Herfurth M, Lindow S, Chreifi G, et al. PilY1 and minor pilins form a complex priming the type IVa pilus in Myxococcus xanthus. Nature Communications. 2020;11(1). doi: 10.1038/s41467-020-18803-z.
8. Ellison CK, Dalia TN, Vidal Ceballos A, Wang JC-Y, Biais N, Brun YV, Dalia AB. Retraction of DNA-bound type IV competence pili initiates DNA uptake during natural transformation in Vibrio cholerae. Nature Microbiology. 2018;3(7):773-80. doi: 10.1038/s41564-018-0174-y.
9. Christman ND, Dalia AB. The molecular basis for DNA-binding by competence T4P is distinct in a representative Gram-positive and Gram-negative species. PLoS Pathog. 2025;21(4):e1013128. Epub 20250421. doi: 10.1371/journal.ppat.1013128. PubMed PMID: 40258067; PubMed Central PMCID: PMCPMC12040237.
10. Guo S, Chang Y, Brun YV, Howell PL, Burrows LL, Liu J. PilY1 regulates the dynamic architecture of the type IV pilus machine in Pseudomonas aeruginosa. Nat Commun. 2024;15(1):9382. Epub 20241030. doi: 10.1038/s41467-024-53638-y. PubMed PMID: 39477930; PubMed Central PMCID: PMCPMC11525922.
11. Barnier J-P, Meyer J, Kolappan S, Bouzinba-Ségard H, Gesbert G, Jamet A, et al. The minor pilin PilV provides a conserved adhesion site throughout the antigenically variable meningococcal type IV pilus. Proceedings of the National Academy of Sciences. 2021;118(45):e2109364118. doi: 10.1073/pnas.2109364118.
12. Cruz LF, Parker JK, Cobine PA, De La Fuente L. Calcium-Enhanced Twitching Motility in Xylella fastidiosa Is Linked to a Single PilY1 Homolog. Appl Environ Microbiol. 2014;80(23):7176-85. Epub 20140912. doi: 10.1128/AEM.02153-14. PubMed PMID: 25217013; PubMed Central PMCID: PMCPMC4249194.
13. Mohandass SN, Collins ACZ, Conradi FD, Allsopp LP, Mullineaux CW. Flocculation of a cyanobacterium confers defense against bacterial predation. bioRxiv. 2025.
14. Mom J, Valette O, Pieulle L, Pelicic V. Unraveling the molecular mechanisms of DNA capture by the Com pilus in naturally transformable monoderm bacteria. mBio. 2025;16(6):e0085125. Epub 20250523. doi: 10.1128/mbio.00851-25. PubMed PMID: 40407325; PubMed Central PMCID: PMCPMC12153270.
15. Ellison TJ, Ellison CK. Improved DNA binding to a type IV minor pilin increases natural transformation. Nucleic Acids Res. 2025;53(10). doi: 10.1093/nar/gkaf467. PubMed PMID: 40444634; PubMed Central PMCID: PMCPMC12123422.
16. Braus SAG, Short FL, Holz S, Stedman MJM, Gossert AD, Hospenthal MK. The molecular basis of FimT-mediated DNA uptake during bacterial natural transformation. Nature Communications. 2022;13(1). doi: 10.1038/s41467-022-28690-1.
17. Hughes-Games A, Davis SA, Hill DJ. Direct visualization of sequence-specific DNA binding by gonococcal type IV pili. Microbiology. 2022;168(8). doi: 10.1099/mic.0.001224.
18. Giltner CL, Habash M, Burrows LL. Pseudomonas aeruginosa Minor Pilins Are Incorporated into Type IV Pili. Journal of Molecular Biology. 2010;398(3):444-61. doi: https://doi.org/10.1016/j.jmb.2010.03.028.
19. Ellison CK, Whitfield GB, Brun YV. Type IV Pili: dynamic bacterial nanomachines. FEMS Microbiol Rev. 2022;46(2). doi: 10.1093/femsre/fuab053. PubMed PMID: 34788436.
20. Hughes HQ, Christman ND, Dalia TN, Ellison CK, Dalia AB. The PilT retraction ATPase promotes both extension and retraction of the MSHA type IVa pilus in Vibrio cholerae. PLoS Genet.

2022;18(12):e1010561. Epub 20221221. doi: 10.1371/journal.pgen.1010561. PubMed PMID: 36542674; PubMed Central PMCID: PMCPMC9815625.
21. Lam T, Ellison CK, Eddington DT, Brun YV, Dalia AB, Morrison DA. Competence pili in Streptococcus pneumoniae are highly dynamic structures that retract to promote DNA uptake. Molecular Microbiology. 2021;116(2):381-96. doi: 10.1111/mmi.14718.
22. Tala L, Fineberg A, Kukura P, Persat A. Pseudomonas aeruginosa orchestrates twitching motility by sequential control of type IV pili movements. Nat Microbiol. 2019;4(5):774-80. Epub 20190225. doi: 10.1038/s41564-019-0378-9. PubMed PMID: 30804544; PubMed Central PMCID: PMCPMC6522360.
23. Ellison CK, Kan J, Chlebek JL, Hummels KR, Panis G, Viollier PH, et al. A bifunctional ATPase drives tad pilus extension and retraction. Sci Adv. 2019;5(12):eaay2591. Epub 20191218. doi: 10.1126/sciadv.aay2591. PubMed PMID: 31897429; PubMed Central PMCID: PMCPMC6920026.
24. Floyd KA, Lee CK, Xian W, Nametalla M, Valentine A, Crair B, et al. c-di-GMP modulates type IV MSHA pilus retraction and surface attachment in Vibrio cholerae. Nat Commun. 2020;11(1):1549. Epub 20200325. doi: 10.1038/s41467-020-15331-8. PubMed PMID: 32214098; PubMed Central PMCID: PMCPMC7096442.
25. Chlebek JL, Dalia TN, Biais N, Dalia AB. Fresh Extension of Vibrio cholerae Competence Type IV Pili Predisposes Them for Motor-Independent Retraction. Applied and Environmental Microbiology. 2021;87(14):e00478-21. doi: doi:10.1128/AEM.00478-21.
26. Chlebek JL, Denise R, Craig L, Dalia AB. Motor-independent retraction of type IV pili is governed by an inherent property of the pilus filament. Proceedings of the National Academy of Sciences. 2021;118(47):e2102780118. doi: 10.1073/pnas.2102780118.
27. Chlebek JL, Hughes HQ, Ratkiewicz AS, Rayyan R, Wang JC-Y, Herrin BE, et al. PilT and PilU are homohexameric ATPases that coordinate to retract type IVa pili. PLOS Genetics. 2019;15(10):e1008448. doi: 10.1371/journal.pgen.1008448.
28. Ellison CK, Dalia TN, Dalia AB, Brun YV. Real-time microscopy and physical perturbation of bacterial pili using maleimide-conjugated molecules. Nat Protoc. 2019;14(6):1803-19. Epub 20190426. doi: 10.1038/s41596-019-0162-6. PubMed PMID: 31028374; PubMed Central PMCID: PMCPMC7461830.
29. Hughes HQ, Floyd KA, Hossain S, Anantharaman S, Kysela DT, Zöldi M, et al. Nitric oxide stimulates type IV MSHA pilus retraction in Vibrio cholerae via activation of the phosphodiesterase CdpA. Proceedings of the National Academy of Sciences. 2022;119(7):e2108349119. doi: 10.1073/pnas.2108349119.
30. Seitz P, Blokesch M. DNA-uptake machinery of naturally competent Vibrio cholerae. Proceedings of the National Academy of Sciences. 2013;110(44):17987-92. doi: 10.1073/pnas.1315647110.
31. Adams DW, Stutzmann S, Stoudmann C, Blokesch M. DNA-uptake pili of Vibrio cholerae are required for chitin colonization and capable of kin recognition via sequence-specific self-interaction. Nat Microbiol. 2019;4(9):1545-57. Epub 20190610. doi: 10.1038/s41564-019-0479-5. PubMed PMID: 31182799; PubMed Central PMCID: PMCPMC6708440.
32. Mom J, Chouikha I, Valette O, Pieulle L, Pelicic V. Systematic functional analysis of the Com pilus in Streptococcus sanguinis: a minimalistic type 4 filament dedicated to DNA uptake in monoderm bacteria. mBio. 2024;15(1):e0266723. Epub 20231214. doi: 10.1128/mbio.02667-23. PubMed PMID: 38095871; PubMed Central PMCID: PMCPMC10790768.
33. Giltner CL, Rana N, Lunardo MN, Hussain AQ, Burrows LL. Evolutionary and functional diversity of the Pseudomonas type IVa pilin island. Environ Microbiol. 2011;13(1):250-64. Epub 20100825. doi: 10.1111/j.1462-2920.2010.02327.x. PubMed PMID: 20738375.
34. Winther-Larsen HC, Wolfgang M, Dunham S, Van Putten JPM, Dorward D, Løvold C, et al. A conserved set of pilin-like molecules controls type IV pilus dynamics and organelle-associated functions in Neisseria gonorrhoeae. Molecular Microbiology. 2005;56(4):903-17. doi: 10.1111/j.1365-2958.2005.04591.x.
35. Yount TA, Porsch EA, St Geme JW, 3rd. Multi-functional minor pilins coordinate type IV pilus assembly, adherence, motility, and DNA uptake in the pediatric pathogen Kingella kingae. mBio. 2025:e0279025. Epub 20251013. doi: 10.1128/mbio.02790-25. PubMed PMID: 41081385.
36. Weaver SJ, Ortega DR, Sazinsky MH, Dalia TN, Dalia AB, Jensen GJ. CryoEM structure of the type IVa pilus secretin required for natural competence in Vibrio cholerae. Nat Commun. 2020;11(1):5080.

Epub 2020/10/10. doi: 10.1038/s41467-020-18866-y. PubMed PMID: 33033258; PubMed Central PMCID: PMCPMC7545093.
37. Oppenheim DS, Yanofsky C. Translational coupling during expression of the tryptophan operon of Escherichia coli. Genetics. 1980;95(4):785-95. doi: 10.1093/genetics/95.4.785. PubMed PMID: 6162715; PubMed Central PMCID: PMCPMC1214269.
38. Tian T, Salis HM. A predictive biophysical model of translational coupling to coordinate and control protein expression in bacterial operons. Nucleic Acids Res. 2015;43(14):7137-51. Epub 20150627. doi: 10.1093/nar/gkv635. PubMed PMID: 26117546; PubMed Central PMCID: PMCPMC4538824.
39. Jain R, Sliusarenko O, Kazmierczak BI. Interaction of the cyclic-di-GMP binding protein FimX and the Type 4 pilus assembly ATPase promotes pilus assembly. PLoS Pathog. 2017;13(8):e1006594. Epub 20170830. doi: 10.1371/journal.ppat.1006594. PubMed PMID: 28854278; PubMed Central PMCID: PMCPMC5595344.
40. Roelofs KG, Jones CJ, Helman SR, Shang X, Orr MW, Goodson JR, et al. Systematic Identification of Cyclic-di-GMP Binding Proteins in Vibrio cholerae Reveals a Novel Class of Cyclic-di-GMP-Binding ATPases Associated with Type II Secretion Systems. PLoS Pathog. 2015;11(10):e1005232. Epub 2015/10/28. doi: 10.1371/journal.ppat.1005232. PubMed PMID: 26506097; PubMed Central PMCID: PMCPMC4624772.
41. Wang Y-C, Chin K-H, Tu Z-L, He J, Jones CJ, Sanchez DZ, et al. Nucleotide binding by the widespread high-affinity cyclic di-GMP receptor MshEN domain. Nature Communications. 2016;7(1):12481-. doi: 10.1038/ncomms12481.
42. Dye KJ, Salar S, Allen U, Smith W, Yang Z. Myxococcus xanthus PilB interacts with c-di-GMP and modulates motility and biofilm formation. J Bacteriol. 2023;205(9):e0022123. Epub 20230911. doi: 10.1128/jb.00221-23. PubMed PMID: 37695853; PubMed Central PMCID: PMCPMC10521364.
43. Hendrix H, Itterbeek A, Longin H, Delanghe L, Vriens E, Vallino M, et al. PlzR regulates type IV pili assembly in Pseudomonas aeruginosa via PilZ binding. Nat Commun. 2024;15(1):8717. Epub 20241008. doi: 10.1038/s41467-024-52732-5. PubMed PMID: 39379373; PubMed Central PMCID: PMCPMC11461919.
44. Koch MD, Fei C, Wingreen NS, Shaevitz JW, Gitai Z. Competitive binding of independent extension and retraction motors explains the quantitative dynamics of type IV pili. Proceedings of the National Academy of Sciences. 2021;118(8):e2014926118. doi: 10.1073/pnas.2014926118.
45. Oliveira NM, Foster KR, Durham WM. Single-cell twitching chemotaxis in developing biofilms. Proc Natl Acad Sci U S A. 2016;113(23):6532-7. Epub 20160524. doi: 10.1073/pnas.1600760113. PubMed PMID: 27222583; PubMed Central PMCID: PMCPMC4988597.
46. Nakane D, Enomoto G, Bähre H, Hirose Y, Wilde A, Nishizaka T. Thermosynechococcus switches the direction of phototaxis by a c-di-GMP-dependent process with high spatial resolution. eLife. 2022;11. doi: 10.7554/elife.73405.
47. Bautista S, Schmidt V, Guiseppi A, Mauriello EMF, Attia B, Elantak L, et al. FrzS acts as a polar beacon to recruit SgmX, a central activator of type IV pili during Myxococcus xanthus motility. EMBO J. 2023;42(1):e111661. Epub 20221108. doi: 10.15252/embj.2022111661. PubMed PMID: 36345779; PubMed Central PMCID: PMCPMC9811614.
48. Kehl-Fie TE, Porsch EA, Miller SE, St Geme JW, 3rd. Expression of Kingella kingae type IV pili is regulated by sigma54, PilS, and PilR. J Bacteriol. 2009;191(15):4976-86. Epub 20090522. doi: 10.1128/JB.00123-09. PubMed PMID: 19465661; PubMed Central PMCID: PMCPMC2715724.
49. Kilmury SL, Burrows LL. Type IV pilins regulate their own expression via direct intramembrane interactions with the sensor kinase PilS. Proc Natl Acad Sci U S A. 2016;113(21):6017-22. Epub 20160509. doi: 10.1073/pnas.1512947113. PubMed PMID: 27162347; PubMed Central PMCID: PMCPMC4889343.
50. Kilmury SLN, Burrows LL. The Pseudomonas aeruginosa PilSR Two-Component System Regulates Both Twitching and Swimming Motilities. mBio. 2018;9(4). Epub 20180724. doi: 10.1128/mBio.01310-18. PubMed PMID: 30042200; PubMed Central PMCID: PMCPMC6058289.
51. Hernandez-Eligio A, Andrade A, Soto L, Morett E, Juarez K. The unphosphorylated form of the PilR two-component system regulates pilA gene expression in Geobacter sulfurreducens. Environ Sci Pollut Res Int. 2017;24(33):25693-701. Epub 20160218. doi: 10.1007/s11356-016-6192-5. PubMed PMID: 26888530.

52. Wu SS, Kaiser D. Regulation of expression of the pilA gene in Myxococcus xanthus. J Bacteriol. 1997;179(24):7748-58. doi: 10.1128/jb.179.24.7748-7758.1997. PubMed PMID: 9401034; PubMed Central PMCID: PMCPMC179738.
53. Hockenberry AM, Hutchens DM, Agellon A, So M. Attenuation of the Type IV Pilus Retraction Motor Influences Neisseria gonorrhoeae Social and Infection Behavior. mBio. 2016;7(6). Epub 20161206. doi: 10.1128/mBio.01994-16. PubMed PMID: 27923924; PubMed Central PMCID: PMCPMC5142622.
54. Schmidt AK, Fitzpatrick AD, Schwartzkopf CM, Faith DR, Jennings LK, Coluccio A, et al. A Filamentous Bacteriophage Protein Inhibits Type IV Pili To Prevent Superinfection of Pseudomonas aeruginosa. mBio. 2022;13(1):e0244121. Epub 20220118. doi: 10.1128/mbio.02441-21. PubMed PMID: 35038902; PubMed Central PMCID: PMCPMC8764522.
55. Taylor VL, Patel PH, Shah M, Yusuf A, Burk CM, Sztanko KM, et al. Prophages block cell surface receptors to preserve their viral progeny. Nature. 2025;644(8078):1049-57. Epub 20250716. doi: 10.1038/s41586-025-09260-z. PubMed PMID: 40670790.
56. Hsiao A, Liu Z, Joelsson A, Zhu J. Vibrio cholerae virulence regulator-coordinated evasion of host immunity. Proc Natl Acad Sci U S A. 2006;103(39):14542-7. Epub 20060918. doi: 10.1073/pnas.0604650103. PubMed PMID: 16983078; PubMed Central PMCID: PMCPMC1599996.
57. Miller VL, DiRita VJ, Mekalanos JJ. Identification of toxS, a regulatory gene whose product enhances toxR-mediated activation of the cholera toxin promoter. J Bacteriol. 1989;171(3):1288-93. doi: 10.1128/jb.171.3.1288-1293.1989. PubMed PMID: 2646275; PubMed Central PMCID: PMCPMC209743.
58. Jaskolska M, Adams DW, Blokesch M. Two defence systems eliminate plasmids from seventh pandemic Vibrio cholerae. Nature. 2022;604(7905):323-9. Epub 20220406. doi: 10.1038/s41586-022-04546-y. PubMed PMID: 35388218; PubMed Central PMCID: PMCPMC7613841.
59. Dalia AB, McDonough E, Camilli A. Multiplex genome editing by natural transformation. Proc Natl Acad Sci U S A. 2014;111(24):8937-42. Epub 20140602. doi: 10.1073/pnas.1406478111. PubMed PMID: 24889608; PubMed Central PMCID: PMCPMC4066482.
60. Dalia AB. Natural Cotransformation and Multiplex Genome Editing by Natural Transformation (MuGENT) of Vibrio cholerae. Methods Mol Biol. 2018;1839:53-64. doi: 10.1007/978-1-4939-8685-9_6. PubMed PMID: 30047054.
61. Schindelin J, Arganda-Carreras I, Frise E, Kaynig V, Longair M, Pietzsch T, et al. Fiji: an open-source platform for biological-image analysis. Nat Methods. 2012;9(7):676-82. Epub 20120628. doi: 10.1038/nmeth.2019. PubMed PMID: 22743772; PubMed Central PMCID: PMCPMC3855844.
62. Ducret A, Quardokus EM, Brun YV. MicrobeJ, a tool for high throughput bacterial cell detection and quantitative analysis. Nat Microbiol. 2016;1(7):16077. Epub 20160620. doi: 10.1038/nmicrobiol.2016.77. PubMed PMID: 27572972; PubMed Central PMCID: PMCPMC5010025.
63. Evans R, O'Neill M, Pritzel A, Antropova N, Senior A, Green T, et al. Protein complex prediction with AlphaFold-Multimer. bioRxiv. 2022:2021.10.04.463034. doi: 10.1101/2021.10.04.463034.
64. Mirdita M, Schutze K, Moriwaki Y, Heo L, Ovchinnikov S, Steinegger M. ColabFold: making protein folding accessible to all. Nat Methods. 2022;19(6):679-82. Epub 20220530. doi: 10.1038/s41592-022-01488-1. PubMed PMID: 35637307; PubMed Central PMCID: PMCPMC9184281.
65. Meng EC, Goddard TD, Pettersen EF, Couch GS, Pearson ZJ, Morris JH, Ferrin TE. UCSF ChimeraX: Tools for structure building and analysis. Protein Sci. 2023;32(11):e4792. doi: 10.1002/pro.4792. PubMed PMID: 37774136; PubMed Central PMCID: PMCPMC10588335.

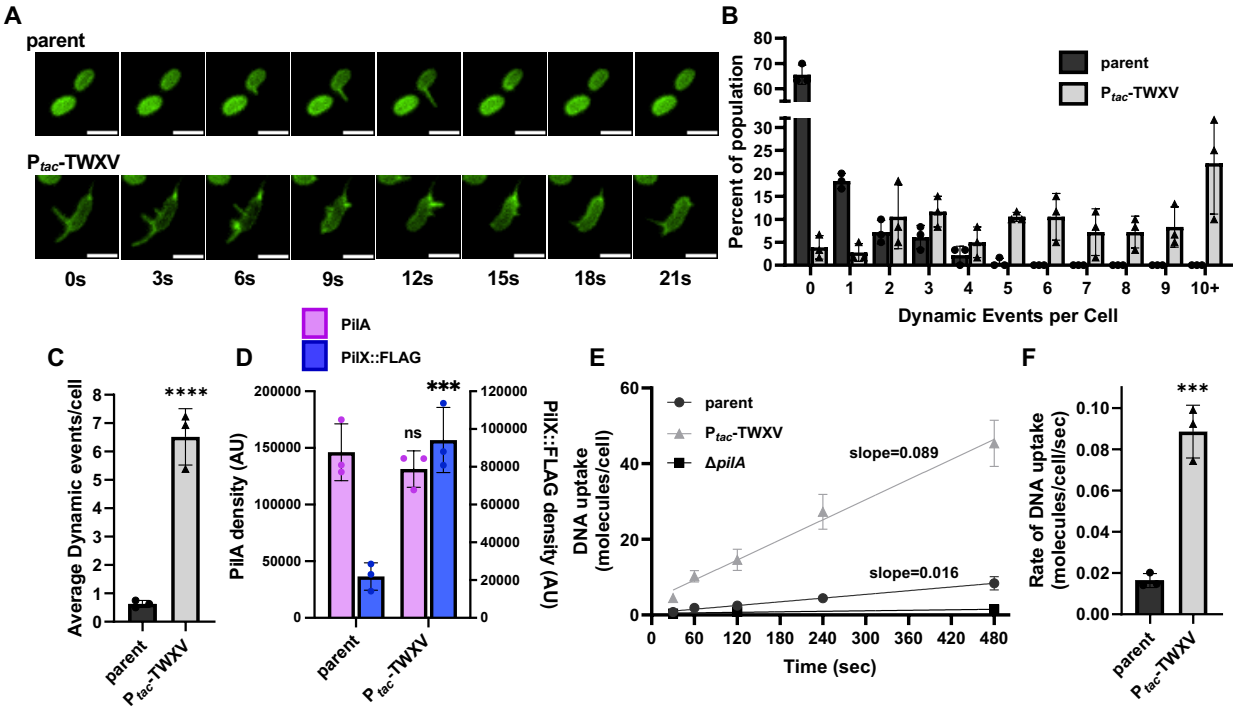

Fig. 1 - Overexpression of minor pilins increases the frequency of T4aP dynamic activity. (**A**) Representative montages of timelapse imaging of AF488-mal labeled cells from the indicated strains. Scale bar, 2 µm. The frequency of T4aP dynamics of the indicated strains was quantified from timelapse imaging of AF488-mal labeled cells (as depicted in **A**) and the (**B**) distribution and (**C**) average dynamics per cell are plotted. (**D**) Quantification of PilA and PilX::FLAG via semi-quantitative western blots of the indicated strains (see **Fig. S4** for standard curves and details). For western blots, the parent strain contained an internally FLAG-tagged allele of *pilX* at the native locus = *pilX*::FLAG; and the P_{tac}-TWXV strain had the same *pilX*::FLAG allele at both the native locus and in the ectopic construct = *pilX*::FLAG P_{tac}-TWX(::FLAG)V. Blots were stained with either α-PilA (purple) or α-FLAG (blue) primary antibodies. (**E**) DNA uptake into the periplasm of the indicated strains was kinetically monitored by qPCR. Lines of best fit were determined by linear regression. The slope of each line is shown, which represents the rate of DNA uptake. (**F**) The rate of DNA uptake of the indicated strains (the slope of the plots depicted in **E**). Data from **B-F** are from 3 independent biological replicates and shown as the mean ± SD. Statistical comparisons were made by unpaired Student's t-test of the log-transformed data. NS, no significance; ** = $p < 0.01$, *** = $p < 0.001$, **** = $p < 0.0001$. Statistical identifiers directly above bars represent comparisons to the parent.

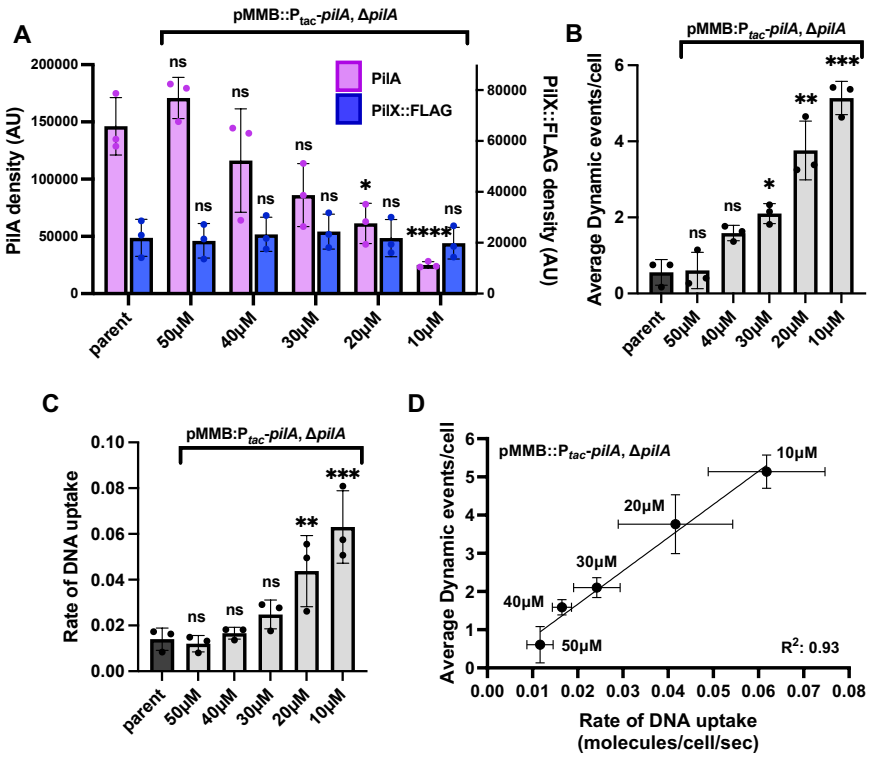

Fig. 2 - The stoichiometry of minor:major pilins regulates the frequency of T4aP dynamic activity. PilA expression was titrated in the pMMB::P_{tac}-*pilA* Δ*pilA* strain via induction of cells at the IPTG concentrations indicated (in μM) in each panel. (**A**) Quantification of PilA and PilX::FLAG via semi-quantitative western blots of the indicated strains (see **Fig. S4** for standard curves and details). For these assays, all strains contained an internally FLAG-tagged allele of *pilX* at the native locus = *pilX*::FLAG. Blots were stained with either α-PilA (purple) or α-FLAG (blue) primary antibodies. The data for the parent is identical to the data shown in **Fig. 1D** and is included here for ease of comparison. (**B**) Quantification of the frequency of T4aP dynamics from timelapse imaging of the indicated strains stained with AF488-mal. (**C**) DNA uptake into the periplasm of the indicated strains was kinetically monitored by qPCR and the rate of DNA uptake was calculated for each replicate and plotted. (**D**) The frequency of dynamic activity in **B** was plotted against the rate of DNA uptake in **C** for the Δ*pilA* pMMB::P_{tac}-*pilA* strain at the indicated doses of IPTG to assess whether these properties are directly correlated. Linear regression analysis was performed and the R^2 value is shown on the plot. All data are from 3 independent biological replicates and shown as the mean ± SD. Statistical comparisons were made by one-way ANOVA with Tukey's multiple comparison test of the log-transformed data. NS = no significance, * = $p < 0.05$, ** = $p < 0.01$, *** = $p < 0.001$, **** = $p < 0.0001$. Statistical identifiers directly above bars represent comparisons to the parent.

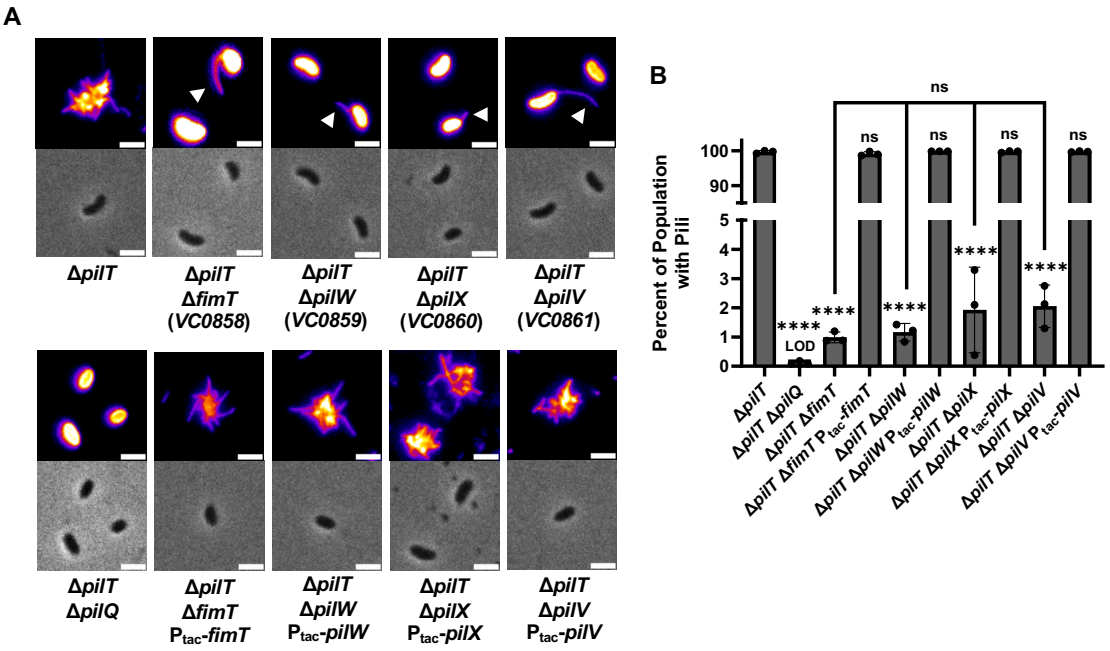

Fig. S1 - VC0858-VC0861 are the core minor pilins of the *V. cholerae* competence T4aP. (**A**) Representative images of the indicated strains stained with AF488-mal. Images are false colored with the "Fire" LUT in Fiji to make rare pili easier to see (white arrows). Scale bar, 2 µm. (**B**) Quantification of surface piliation in the indicated strains stained with AF488-mal, as depicted in **A**. Data in **B** is from 3 independent biological replicates and shown as the mean ± SD. The number of cells quantified varied for each strain and replicate. The total number of cells analyzed for each strain: Δ*pilT* = 2478, Δ*pilT* Δ*pilQ* = 2917, Δ*pilT* Δ*fimT* = 4003, Δ*pilT* Δ*pilW* = 3331, Δ*pilT* Δ*pilX* = 3791, Δ*pilT* Δ*pilV* = 3233, Δ*pilT* Δ*fimT* P_{tac}-*fimT* = 2483, Δ*pilT* Δ*pilW* P_{tac}-*pilW* = 2489, Δ*pilT* Δ*pilX* P_{tac}-*pilX* = 2560, Δ*pilT* Δ*pilV* P_{tac}-*pilV* = 3011. Statistical comparisons were made by one-way ANOVA with Tukey's multiple comparison test of the log-transformed data. NS, no significance; **** = $p < 0.0001$. LOD, limit of detection. Statistical identifiers directly above bars represent comparisons to the Δ*pilT* parent.

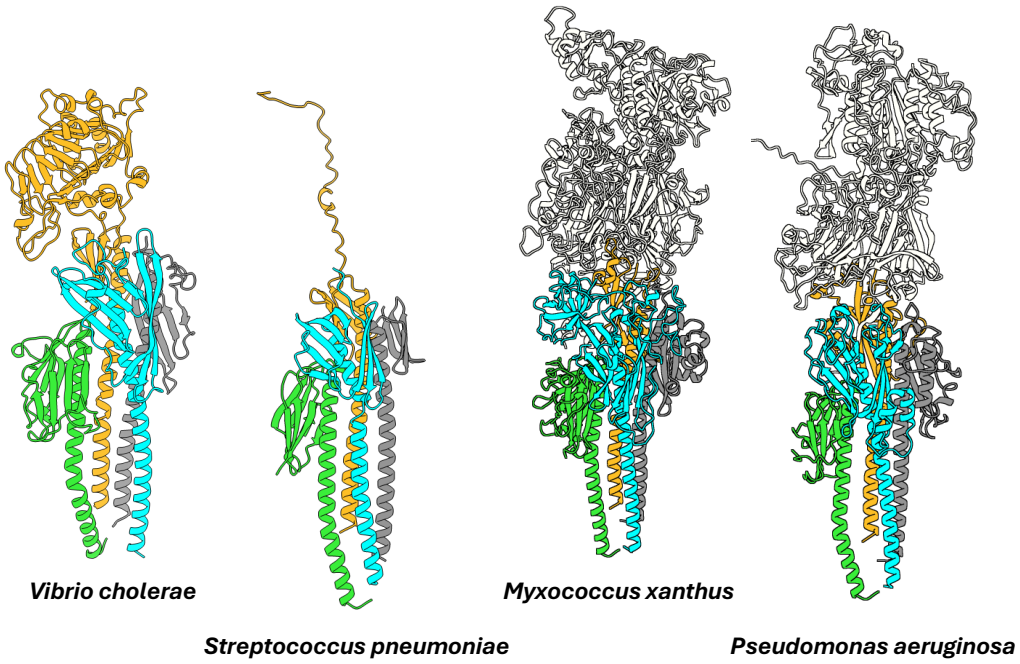

Fig. S2 - *V. cholerae* core minor pilins were named based on their structural homology to established T4aP. AlphaFold-multimer models of the core minor pilins from *V. cholerae*, *S. pneumoniae*, *M. xanthus*, and *P. aeruginosa*. Pilins are colored based on their structure and position within the predicted complex. Green = FimU/T, Cyan = PilW, Grey = PilV, Yellow = PilX. For both *M. xanthus* and *P. aeruginosa*, PilY1 is included in white.

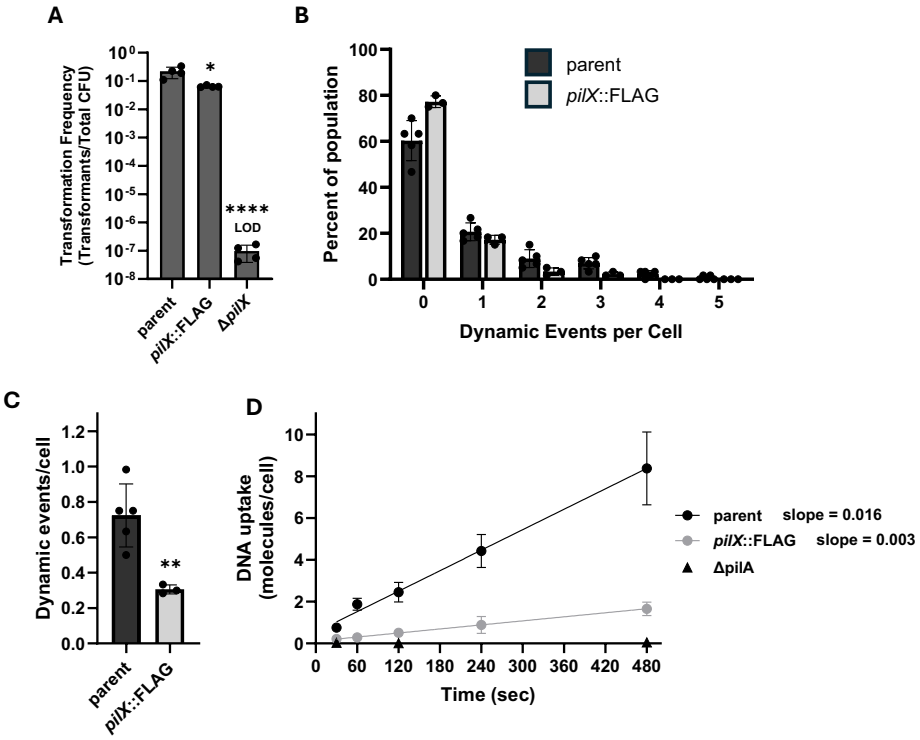

Fig. S3 - PilX::FLAG is functional but exhibits slightly reduced dynamic activity. (**A**) Transformation assays of the indicated strains. (**B**-**C**) The frequency of T4aP dynamics of the indicated strains was quantified from timelapse imaging of AF488-mal labeled cells and the (**B**) distribution and (**C**) average T4aP dynamics per cell are plotted. Parent data shown here are identical to data shown in **Fig. 1B and 1C** and included for ease of comparison. (**D**) DNA uptake into the periplasm of the indicated strains was kinetically monitored by qPCR. Parent and Δ*pilA* data shown here are identical to data shown in **Fig. 1E** and included for ease of comparison. Lines of best fit were determined by linear regression. The slope of each line is shown, which represents the rate of DNA uptake. Data is from at least 3 independent biological replicates and shown as the mean ± SD. Statistical comparisons were made in **A** by one-way ANOVA with Tukey's multiple comparison test of the log-transformed data, and in **C** by unpaired Student's t-test of the log-transformed data. * = $p < 0.05$, ** = $p < 0.01$, **** = $p < 0.001$. LOD = limit of detection. Statistical identifiers directly above bars represent comparisons to the parent.

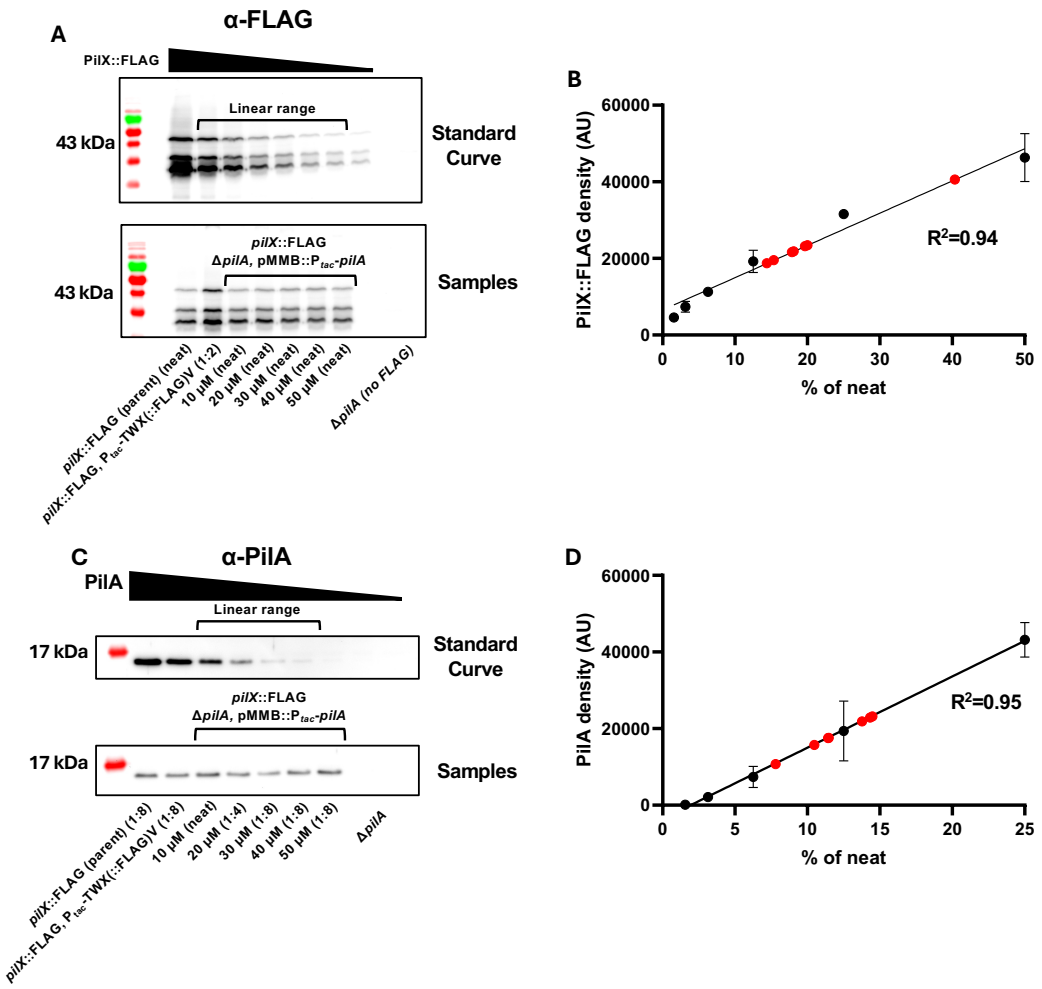

Fig. S4 – Assessing minor and major pilin levels via semi-quantitative western blots. (**A**) Representative semi-quantitative western blots for detecting PilX::FLAG using α-FLAG primary antibodies. A serial 2-fold dilution series of PilX::FLAG (*i.e.,* dilutions of a *pilX*::FLAG P_{tac}-TWX(::FLAG)V lysate) (top) was used to generate a standard curve to define the linear range of the assay. Experimental samples (bottom) from the indicated strains were diluted (dilution factor noted in parentheses) and blotted so that the signal would be within the linear range of the assay. PilX::FLAG is 45 kDa, and the size of the closest ladder band is demarcated to the left of the blot. (**B**) Blots, as shown in **A**, were analyzed by densitometry and plotted. Black datapoints correspond to the standard curve (n = 3), and only data points within the linear range are shown. Linear regressions show the line of best fit for the standard curve and the R^2 is shown on the plot. Red datapoints correspond to the densities of the experimental samples in **A**, and highlight that these data are within the linear range of the assay. (**C**) Representative semi-quantitative western blots for detecting PilA via α-PilA antibodies. A 2-fold dilution series of PilA (*i.e.*, dilutions of a Δ*pilA* pMMB::P_{tac}-*pilA* lysate) (top) was used to generate a standard curve to define the linear range of the assay. Experimental samples (bottom) from the indicated strains were diluted (dilution factor noted in parentheses) and blotted so that the signal would be within the linear range of the assay. (**D**) Blots, as shown in **C**, were analyzed by densitometry and plotted. Black datapoints correspond to the standard curve (n = 3), and only data points within the linear range are shown. Linear regressions show the line of best fit for the standard curve and the R^2 is shown on the plot. Red datapoints correspond to the densities of the experimental samples in **C** and highlight that these data are within the linear range of the assay. PilA is 15 kDa, and the size of the closest ladder band is demarcated to the left of the blot.

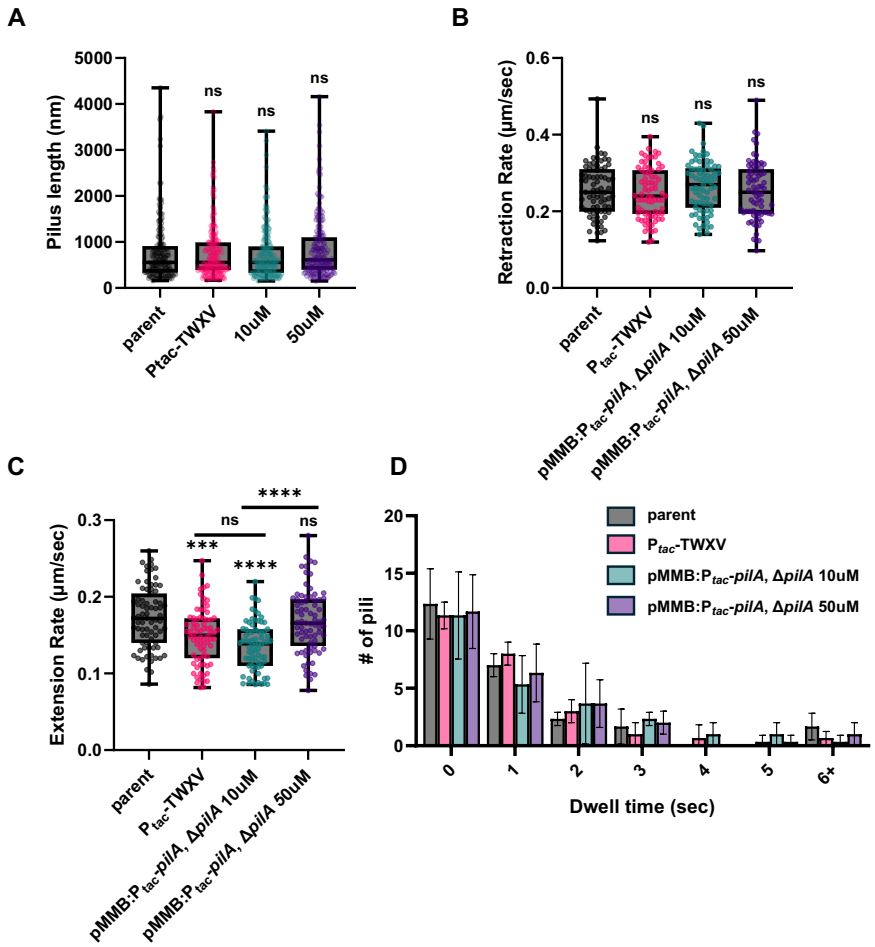

Fig. S5 - The minor:major pilin ratio does not affect other properties of T4aP dynamics. Timelapse imaging was performed on AF488-mal labeled cells of the indicated strains and images were analyzed to determine the following properties of T4aP dynamics. (**A**) Maximum pilus lengths. (**B**) The rate of pilus retraction. (**C**) The rate of pilus extension. (**D**) The dwell time for pili. Dwell time is defined as the amount of time before an extended pilus begins to retract. Data are from 3 independent biological replicates and shown as the mean ± SD. Statistical comparisons were made by one-way ANOVA with Tukey's multiple comparison test of the log-transformed data. ns = no significance, *** = $p < 0.001$, **** = $p < 0.0001$. Statistical identifiers directly above bars represent comparisons to the parent.

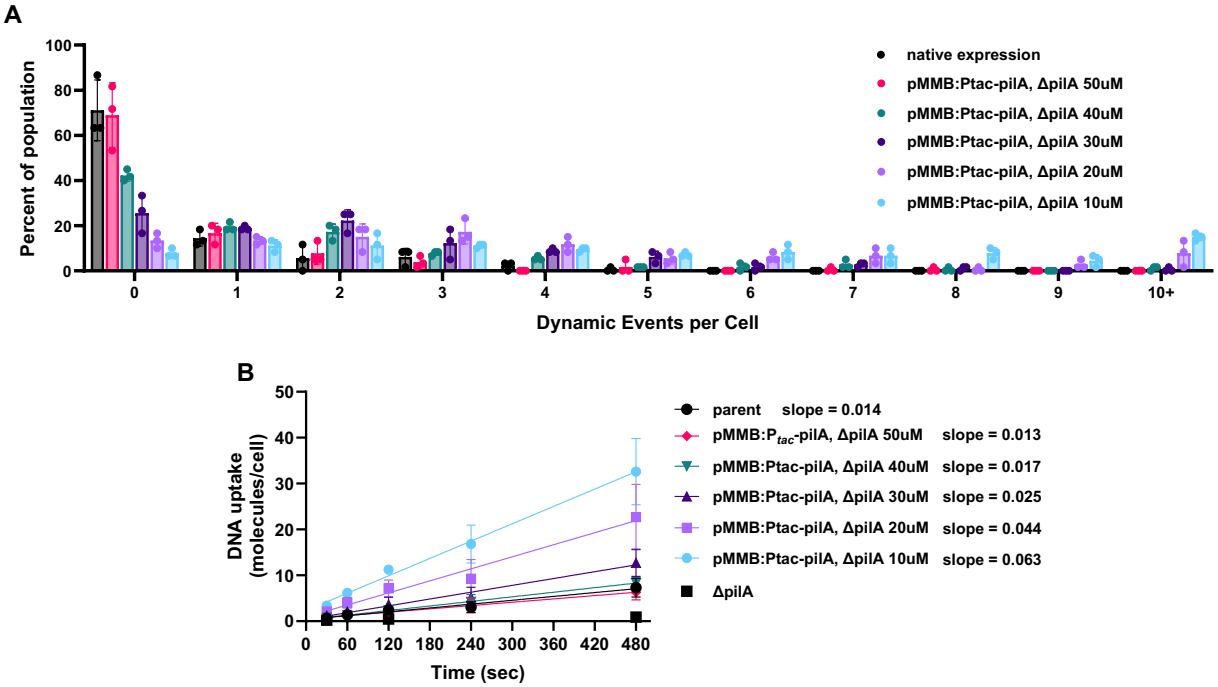

Fig. S6 - Quantification of the frequency of T4aP dynamic activity and DNA uptake when underexpressing PilA. (**A**) Quantification of the frequency of T4aP dynamics from timelapse imaging of the indicated strains stained with AF488-mal. (**B**) DNA uptake into the periplasm of the indicated strains was kinetically monitored by qPCR. Lines of best fit were determined by linear regression. The slope of each line is shown, which represents the rate of DNA uptake. Data are from 3 independent biological replicates and shown as the mean ± SD.

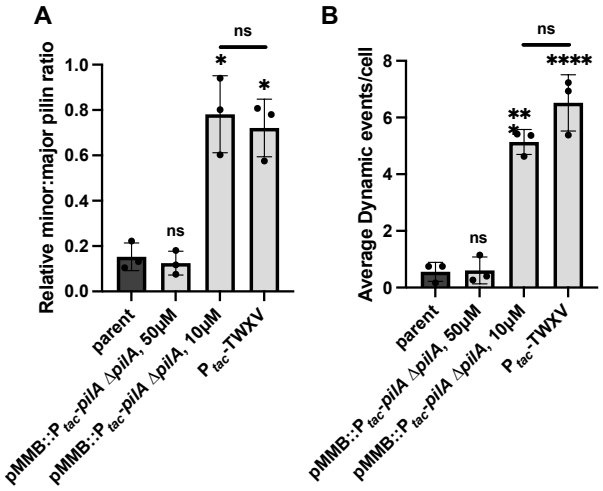

Fig. S7 - Altering the minor:major pilin ratio by overexpressing minor pilins vs underexpressing the major pilin has the same effect on T4aP dynamics. (**A**) The minor:major pilin ratio of the indicated samples was determined by semi-quantitative western blots. For these assays, all strains contained an internally FLAG-tagged allele of *pilX* at the native locus = *pilX*::FLAG; and the P_{tac}-TWXV strain had the same *pilX*::FLAG allele at both the native locus and in the ectopic construct = *pilX*::FLAG P_{tac}-TWX(::FLAG)V. For each sample, the relative PilX::FLAG density was divided by the relative PilA density using the data presented in **Fig. 1D** and **Fig. 2A**. Notably, because PilA and PilX::FLAG were quantified using distinct antibodies, this ratio does not signify the absolute minor:major pilin ratio, but rather the relative minor:major pilin ratio. (**B**) Quantification of the frequency of T4aP dynamics from timelapse imaging of the indicated strains stained with AF488-mal. All data are identical to the results presented in **Fig. 1C** and **2B** and are shown here for ease of comparison. All data are from 3 independent biological replicates and shown as the mean ± SD. Statistical comparisons were made by one-way ANOVA with Tukey's multiple comparison test of the log-transformed data. ns = no significance, * = $p < 0.05$, *** = $p < 0.001$, **** = $p < 0.0001$. Statistical identifiers directly above bars represent comparisons to the parent.

763 **Table S1** – *Strains used in this manuscript*
764

Strain #	Genotype	Figures	Use in manuscript
NDC0547 / SAD4071	Δ*pilT*::*Tm*^{R}, Δ*VC1807*::*Zeo*^{R}, P_{const2}-*tfoX*, Δ*luxO*, *lacZ*::*lacI*^{q}, *pilA*^{S67C}	Fig. S1	Parent for surface piliation microscopy and quantification
NDC0585 / SAD4072	Δ*pilQ*::*Tet*^{R}, Δ*pilT*::*Tm*^{R}, Δ*VC1807*::*Zeo*^{R}, P_{const2}-*tfoX*, Δ*luxO*, *lacZ*::*lacI*^{q}, *pilA*^{S67C}	Fig. S1	Δ*pilQ* control for surface piliation microscopy and quantification
NDC0575 / SAD4073	Δ*fimT,* Δ*lacZ*::*Spec*^{R}, Δ*pilT*::*Tm*^{R}, Δ*VC1807*::*Zeo*^{R}, P_{const2}-*tfoX*, Δ*luxO*, *lacZ*::*lacI*^{q}, *pilA*^{S67C}	Fig. S1	Δ*fimT* for surface piliation microscopy and quantification
NDC0758 / SAD4074	Δ*pilW,* Δ*lacZ*::*Spec*^{R}, Δ*pilT*::*Tm*^{R}, Δ*VC1807*::*Kan*^{R}, P_{const2}-*tfoX*, Δ*luxO*, *lacZ*::*lacI*^{q}, *pilA*^{S67C}	Fig. S1	Δ*pilW* for surface piliation microscopy and quantification
NDC0749 / SAD4075	Δ*pilX,* Δ*lacZ*::*Spec*^{R}, Δ*pilT*::*Tm*^{R}, Δ*VC1807*::*Kan*^{R}, P_{const2}-*tfoX*, Δ*luxO*, *lacZ*::*lacI*^{q}, *pilA*^{S67C}	Fig. S1, S3	Δ*pilX* for surface piliation microscopy and quantification
NDC0751 / SAD4076	Δ*pilV,* Δ*lacZ*::*Spec*^{R}, Δ*pilT*::*Tm*^{R}, Δ*VC1807*::*Kan*^{R}, P_{const2}-*tfoX*, Δ*luxO*, *lacZ*::*lacI*^{q}, *pilA*^{S67C}	Fig. S1	Δ*pilV* for surface piliation microscopy and quantification
NDC0576 / SAD4077	Δ*lacZ*::Tet^R-*lacI*-P_{tac}-*fimT*, Δ*fimT,* Δ*pilT*::*Tm*^{R}, Δ*VC1807*::*Zeo*^{R}, P_{const2}-*tfoX*, Δ*luxO*, *lacZ*::*lacI*^{q}, *pilA*^{S67C}	Fig. S1	Δ*fimT* complement for surface piliation microscopy and quantification
NDC0752 / SAD4078	Δ*lacZ*::Tet^R-*lacI*-P_{tac}-*PilW*, Δ*pilW,* Δ*pilT*::*Tm*^{R}, Δ*VC1807*::*Zeo*^{R}, P_{const2}-*tfoX*, Δ*luxO*, *lacZ*::*lacI*^{q}, *pilA*^{S67C}	Fig. S1	Δ*pilW* complement for surface piliation microscopy and quantification
NDC0754 / SAD4079	Δ*lacZ*::Tet^R-*lacI*-P_{tac}-*PilX*, Δ*pilX,* Δ*pilT*::*Tm*^{R}, Δ*VC1807*::*Zeo*^{R}, P_{const2}-*tfoX*, Δ*luxO*, *lacZ*::*lacI*^{q}, *pilA*^{S67C}	Fig. S1	Δ*pilX* complement for surface piliation microscopy and quantification
NDC0755 / SAD4080	Δ*lacZ*::Tet^R-*lacI*-P_{tac}-*PilV*, Δ*pilV,* Δ*pilT*::*Tm*^{R}, Δ*VC1807*::*Zeo*^{R}, P_{const2}-*tfoX*, Δ*luxO*, *lacZ*::*lacI*^{q}, *pilA*^{S67C}	Fig. S1	Δ*pilV* complement for surface piliation microscopy and quantification
NDC0713 / SAD4081	PilX G244::3xFLAG, Δ*ddmABC*::*Erm*^{R}, Δ*ddmDE*::*Kan*^{R} Δ*VC1807*::*Cm*^{R}, P_{const2}-*tfoX*, Δ*luxO*, *lacZ*::*lacI*^{q}, *pilA*^{S67C}	Fig. 1D, 2A, S3, S4, S7	"native expression" for internally FLAG-tagged PilX (inserted after residue G244) for western blotting.
NDC0719 / SAD4082	Δ*lacZ*::Tet^R-*lacI*-P_{tac}-*TWX(3xFLAG)V,* PilX G244::3xFLAG, Δ*ddmABC*::*Erm*^{R}, Δ*ddmDE*::*Kan*^{R} Δ*VC1807*::*Cm*^{R}, P_{const2}-*tfoX*, Δ*luxO*, *lacZ*::*lacI*^{q}, *pilA*^{S67C}	Fig. 1D, S3, S4, S7	Minor pilin overexpression strain for western blotting. The internal FLAG tag is present in both the native and ectopic copies of PilX.
NDC0761 / SAD4083	Δ*pilA*, Δ*ddmABC*::*Erm*^{R}, Δ*ddmDE*::*Kan*^{R} Δ*VC1807*::*Tm*^{R}, P_{const2}-*tfoX*, Δ*luxO*, *lacZ*::*lacI*^{q}, *pilA*^{S67C}	Fig. 1D, 1E, S4, S6	Δ*pilA* and “NO FLAG” control for western blotting and DNA uptake assays
NDC0707 / SAD4084	Δ*ddmABC*::*Erm*^{R}, Δ*ddmDE*::*Kan*^{R} Δ*VC1807*::*Zeo*^{R}, P_{const2}-*tfoX*, Δ*luxO*, *lacZ*::*lacI*^{q}, *pilA*^{S67C}	Fig. 1A-C,1E-F, 2B-C, S3, S5, S6, S7	parent/"native expression" for measuring dynamic activity, DNA uptake, pilus length, pilus dwell time, and pilus extension/retraction rates
NDC0746 / SAD4085	Δ*lacZ*::Tet^R-*lacI*-P_{tac}-*TWXV*, Δ*ddmABC*::*Erm*^{R}, Δ*ddmDE*::*Kan*^{R} Δ*VC1807*::*Zeo*^{R}, P_{const2}-*tfoX*, Δ*luxO*, *lacZ*::*lacI*^{q}, *pilA*^{S67C}	Fig. 1A-C, 1E-F, S5, S7	Minor pilin overexpression strain for measuring dynamic activity, DNA uptake, pilus length, pilus dwell time, and pilus extension/retraction rates

NDC0763 / SAD4086	pMMB::P_{tac}-*pilA* *Spec*^{R} *Carb*^{R}, Δ*pilA*, PilX G244::3xFLAG, Δ*ddmABC*::*Erm*^{R}, Δ*ddmDE*::*Kan*^{R} Δ*VC1807*::*Cm*^{R}, P_{const2}-*tfoX*, Δ*luxO*, *lacZ*::*lacI*^{q}, *pilA*^{S67C}	Fig. 2A, S4, S7	Major pilin titratable expression strain for western blotting
NDC0730 / SAD4087	pMMB::P_{tac}-*pilA* *Spec*^{R} *Carb*^{R}, Δ*pilA*, Δ*ddmABC*::*Erm*^{R}, Δ*ddmDE*::*Kan*^{R} Δ*VC1807*::*Cm*^{R}, P_{const2}-*tfoX*, Δ*luxO*, *lacZ*::*lacI*^{q}, *pilA*^{S67C}	Fig. 2B-D, S5, S6, S7	Major pilin titratable expression strain for measuring dynamic activity, DNA uptake, pilus length, pilus dwell time, and pilus extension/retraction rates

765
766

767 **Table S2** – *Primers used in this study*
768

Primer #	Sequence	Use
DOG0400	ACTTCTGGCTGAAGGTCAATTTTC	Δ*pilT* F1
DOG0401	gtcgacggatccccggaatCATTTAAATTCCTTAATAAAGTCTGGC	Δ*pilT* R1
DOG0402	gaagcagctccagcctacaTAGGTAGGTAAAGACAGATGGAG	Δ*pilT* F2
DOG0403	TCACGTGTTCGGCCAAAATC	Δ*pilT* R2
DOG0404	TTCTGCTTGCCTTGCGTC	Δ*pilT* detect
DOG0582	ACATCTGGCAGATCTGATTTCAC	Δ*pilQ* F1
DOG0583	gtcgacggatccccggaatCAACCGATTATTTTAAAGCCAGCTTG	Δ*pilQ* R1
DOG0584	gaagcagctccagcctacaTAACTTAGCGTGTGCGTAACAAG	Δ*pilQ* F2
DOG0585	TTGTGTTTGCTCTAACGTTTGC	Δ*pilQ* R2
DOG0586	ACAAGAGTTGCTGGACATACG	Δ*pilQ* detect
DOG0549	AACGACATTACTGACGTTATCCTAG	Δ*fimT* F1
DOG0550	gtcgacggatccccggaatATGCATTTCCCAAAATCCTTTGC	Δ*fimT* R1
DOG0551	gaagcagctccagcctacaGCTGGACGAATCAAAGTTTGC	Δ*fimT* F2
DOG0552	AATGATACCGCCCAGAGGAATC	Δ*fimT* R2
DOG0553	ATCACACCGACAGCACCA	Δ*fimT* detect
DOG0554	gtcgacggatccccggaatTTGCTGGTTAGCACTTTTCAAAGC	Δ*pilW* R1
DOG0555	gaagcagctccagcctacaGCTATCTCATTACAGGTTCAGC	Δ*pilW* F2
DOG0556	TCGAACATAAATATCAGAAGCTGA	Δ*pilW* detect
DOG0557	TGGTGACTGAGAACATGTCAAAAC	Δ*pilX* F1
DOG0558	gtcgacggatccccggaatAATCATTATTTCCAATTCCTTTGCTG	Δ*pilX* R1
DOG0559	gaagcagctccagcctacaGATGTGATCGATCATATTGCGAG	Δ*pilX* F2
DOG0560	TCATCGTGCATTTGTCCAGTTAAG	Δ*pilX* R2
DOG0561	ATGAGTTTGCACTTATCAGCG	Δ*pilX* detect
DOG0562	gtcgacggatccccggaatACCAGATTGCTTATTGCGC	Δ*pilV* R1
DOG0563	gaagcagctccagcctacaTGAACGAGTCCTTCTTGCC	Δ*pilV* F2
DOG0564	TAGTGATAAAGCCTGAAGAGTCAG	Δ*pilV* detect
BBC1944	caatttcacacaggatcccgggAGGAGGTTGGGAAATGCATCGCGGCTTTAC	P_{tac}-*fimT* F
BBC1945	tgtaggctggagctgcttcGGTTAGCACTTTTCAAAGCCATA	P_{tac}-*fimT* R
BBC1946	caatttcacacaggatcccgggAGGAGGTCAAAATATGGCTTTGAAAAGTGC	P_{tac}-*pilW* F
BBC1947	tgtaggctggagctgcttcTTATTTCCAATTCCTTTGCTGAACC	P_{tac}-*pilW* R
BBC1948	caatttcacacaggatcccgggAGGAGGTGAAATAATGATTCAATATCAAAAAGGTGTC	P_{tac}-*pilX* F
BBC1949	tgtaggctggagctgcttcTTATTGCGCATTCCAGCTTC	P_{tac}-*pilX* R
BBC1950	caatttcacacaggatcccgggAGGAGGTGCTGGAATGCGCAATAAGC	P_{tac}-*pilV* F
BBC1951	tgtaggctggagctgcttcTCAGTCAAATTCGCTGTATTTAGAG	P_{tac}-*pilV* R
DOG0548	AAGAGTTTGAAGAGTCTTGTGGC	*pilX* G244::3xFLAG F1
NCP0229	tccaccacttccacctgcACCATTCGTATTTTCTGGAGC	*pilX* G244::3xFLAG R1
NCP0230	gcaggtggagcaggtggaCAACCTAGTATTGTTCCTGATTG	*pilX* G244::3xFLAG F2
BBC1874	GAGACGCTGACAAAATCACAC	*pilX* G244::3xFLAG R2
BBC993	ttgattataaggatgacgatgac	*pilX* G244::3xFLAG detect F
NCP0239	CTCGCAATATGATCGATCACATC	*pilX* G244::3xFLAG detect R
NCP0486	caatttcacacaggatcccgggTTTGCAAAGGATTTTGGGAAATG	P_{tac}-*TWXV* F
DOG0565	AGATTGGTCTATTTTATGGCTCAAG	Δ*pilA* F1

DOG0566	gtcgacggatccccggaatCATATGCCTTGCTACACAAGG	Δ*pilA* R1
DOG0567	gaagcagctccagcctacaCCAAAAGGCTGTACTGCAGG	Δ*pilA* F2
DOG0568	AGGGTCAGTTTACCCTCTGG	Δ*pilA* R2
DOG0569	TACTTAACTCAAGCAGCGCC	Δ*pilA* detect
BBC4286	AGATATAGCGAATGACCGTTTGC	Δ*ddmABC* F1
BBC4287	gtcgacggatccccggaatCATTCAACCTCTTATGAAATCATACC	Δ*ddmABC* R1
BBC4288	gaagcagctccagcctacaCCGCTGGATTGGCTATAAAGC	Δ*ddmABC* F2
BBC4289	AAGATAGCGCAGAGCTTCAG	Δ*ddmABC* R2
BBC4290	AGCTTACTTGACCCATTGTCTG	Δ*ddmABC* detect
BBC4212	ATGGAACCGAAACGTGATCAG	Δ*ddmDE* F1
BBC4213	gtcgacggatccccggaatGAACATGTCGAATAACTAGACAGG	Δ*ddmDE* R1
BBC4214	gaagcagctccagcctacaTGATAGCAGACTAAACCACGG	Δ*ddmDE* F2
BBC4215	TCAGCAATTAAGCCTTCCG	Δ*ddmDE* R2
BBC4216	GTTTGTTATGTACTGAGTGGTCC	Δ*ddmDE* detect
JCP313	caatttcacacaggatcccgggAGGAGGTGAAATTATGAAAGCG	P_{tac}-*pilA* F
BBC1884	tgtaggctggagctgcttcTTAGTTAATTGTTGCACCTGC	P_{tac}-*pilA* R
BBC2822	aatttcacacaggaaacagaattcgagctcTTGTTTCGGCGTGGGTATGGTG	To clone P_{tac}-*pilA* onto pMMB F
BBC2823	caggtcgactctagaggatccccgggtacCtgtaggctggagctgcttc	To clone P_{tac}-*pilA* onto pMMB R
BBC2824	gagctcgaattctgtttcctgtgtgaaattTTTGCCAGAACCGTTATGATGTC	pMMB F
BBC2357	GGTACCCGGGGATCCTCTAGAGTCGACCTGCAGGCATGCAAGCTTGGC	pMMB R

769